Periodica Polytechnica
Civil Engineering

OnlineFirst (2018) paper 11916
https://doi.org/10.3311/PPci.11916

Fracture Propagation in Brazilian Discs with Multiple Pre-existing Notches by Using a Phase Field Method

Shuwei Zhou[1,2*]

RESEARCH ARTICLE

Received 30 July 2017; Revised 13 February 2017; Accepted 22 February 2018

Abstract

The crack propagation in the Brazilian discs with multiple pre-existing notches is investigated by using a phase field method. The phase field modeling is verified by applying a direct tension test and an indirect splitting test on a Brazilian specimen with no pre-existing notches where the simulated results are in good agreement with previous numerical and experimental results. The influence of the notch number and spacing on the crack propagation in the Brazilian discs with multiple vertically and horizontally arranged notches is studied. Outer cracks initiate from the notch tips and propagate at a small angle with the vertical direction, finally coalescing with the ends of the discs. The strength of the specimen decreases as the notches increases. The Brazilian discs with horizontally arranged pre-existing notches only have outer cracks when the notch number is 1, 3, and 5 and have both outer and inner cracks for two and four notches. The peak load of the Brazilian discs with horizontally arranged notches increases as the notch spacing increases. The final crack patterns obtained by the phase field modeling are consistent with those by previous numerical simulations and experimental tests.

Keywords

phase field method, Brazilian disc, multiple notches

1 Department of Geotechnical Engineering,
College of Civil Engineering,
Tongji University,
Shanghai 200092, P.R. China
2 Institute of Structural Mechanics,
Bauhaus-University Weimar,
Weimar 99423, Germany
* Corresponding author, email: zhoushuwei1016@126.com

1 Introduction

Natural rocks contain abundant cracks and usually show heterogeneity. Under loading, cracks initiate, propagate, and coalesce with other cracks, thereby decreasing the strength of rocks. The initiation and propagation of multiple cracks significantly affect many rock engineering problems, such as rock cutting, hydraulic fracturing, and explosive fracturing [1]. In the past decades, crack propagation in rocks has received attentions from many researches [2–5], among which many novel tests were applied to investigate crack patterns under compressive loads, such as the notched semi-circular bending tests (NSCB) [6], the cracked chevron notched semi-circular bending method (CCNSCB) [7], and the Brazil splitting tests [8].

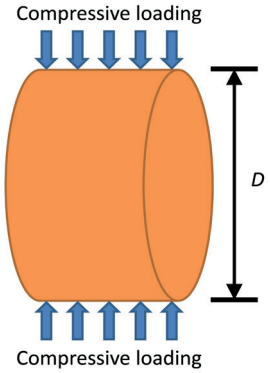

Fig. 1 The Brazilian test

The Brazilian disc test (Fig. 1) is among the most effective tests for fracture mechanism in rocks. The Brazilian disc specimen containing a central pre-existing notch is commonly used to determine the static and dynamic fracture toughness of a rock. For example, researchers [9] estimated the mixed Mode I/II fracture toughness of rocks by using the cracked straight through Brazilian disk (CSTBD) specimens. However, the knowledge is still limited for understanding the fracture mechanism in the Brazilian discs with multiple pre-existing cracks and some preliminary works are conducted in recent years [10–13]. These studies basically used the numerical methods to model fracture initiation and propagation and then concluded the fracture mechanism because preparation of the

Brazilian discs with multiple pre-existing cracks is difficult in experimental tests [10]. For example, Haeri et al. [11] used the displacement discontinuity method (DDM) to simulate crack propagation in Brazilian discs with multiple notches. Sarfarazi et al. [12] applied the particle flow code (PFC) and compared the PFC simulations with the results by using DDM.

In this paper, an effective numerical tool for crack simulation namely, the phase field method (PFM) is used to study crack initiation and propagation in Brazilian discs with multiple pre-existing notches. The advantages of the PFM are manifold: i) the crack propagation simulation has strict physical meaning, ii) crack propagation path is automatically obtained without any external criteria to tackle crack surfaces, and iii) PFM has a good prediction of complex fractures, such as crack coalescence and branching. The phase field method has been extensively tested after it was proposed. For example, Robertson [13] examined and compared the PFM simulation with the experimental data.

In addition, the phase field method used in this paper is verified by a direct tension test and a Brazilian splitting test on a specimen without pre-existing notches. The influence of notch number and spacing on the crack propagation in the Brazilian discs with multiple horizontally and vertically arranged notches is studied. We also compare the crack patterns obtained by the PFM with those of previous numerical simulations and experimental tests.

This paper is outlined as follows. Section 2 presents the phase field method for fracture and Section 3 gives the details of finite element implementation. Section 4 verifies the phase field method by a benchmark example of direct tension test and a Brazil splitting test on a specimen with no pre-existing cracks. Section 5 shows the influence of the notch number and spacing on the crack propagation in the Brazilian discs with vertically arranged notches, while Section 6 is for the horizontally arranged notches. Section 7 concludes this paper.

2 Phase field method for fracture

The phase field method for fracture in this paper is based on the variational principle proposed by [14]. In Fig. 2a, we consider a brittle domain Ω, which is bounded by the surface $\partial\Omega$. Γ is the crack set. The variational principle requires minimization of the energy functional L:

$$L(\boldsymbol{u},\Gamma)=\int_\Omega \psi(\boldsymbol{\varepsilon})\mathrm{d}\Omega+\int_\Gamma G_c\mathrm{d}S-\int_\Omega \boldsymbol{b}\cdot\boldsymbol{u}\mathrm{d}\Omega-\int_{\partial\Omega_h}\boldsymbol{t}\cdot\boldsymbol{u}\mathrm{d}S \quad (1)$$

with $\boldsymbol{u}$ the displacement field. In addition, G_c is the critical energy release rate. $\boldsymbol{b}$ and $\boldsymbol{t}$ are the body force and surface traction, respectively. $\psi(\boldsymbol{\varepsilon})$ is the elastic energy with $\boldsymbol{\varepsilon}$ the linear strain tensor given by

$$\varepsilon_{ij}=\frac{1}{2}\left(u_{i,j}+u_{j,i}\right). \quad (2)$$

The energy functional in Eq. (1) cannot be directly minimized because the displacement is discontinuous and the crack set is unknown. Therefore, an auxiliary scalar field ϕ (phase field) is used to approximate the sharp crack surface in Fig. 2b. We define that $\phi = 0$ represents the unbroken material and $\phi = 1$ the fully broken one. According to Miehe et al. [15, 16], one has

$$\int_\Gamma G_c\mathrm{d}S=\int_\Omega\frac{G_c}{2l_0}\left(\phi^2+l_0^2\phi_{,i}\phi_{,i}\right)\mathrm{d}\Omega \quad (3)$$

with l_0 the length scale parameter that reflects the shape of a crack. The mushy crack region will have a larger width with a larger l_0.

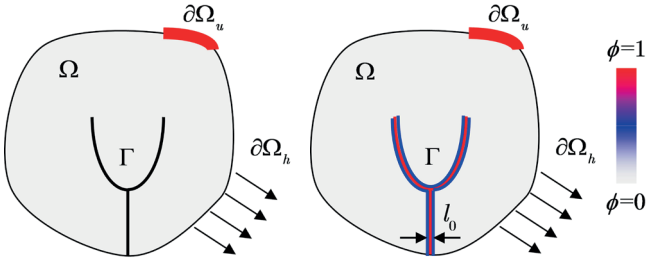

(a) Sharp crack set (b) Mushy crack set

Fig. 2 Phase field approximation of the sharp crack set

To ensure the fracture initiation and propagation only under tension, the strain requires decomposition. Here, we define operators $\langle\cdot\rangle_+=(\cdot+|\cdot|)/2$ and $\langle\cdot\rangle_-=(\cdot-|\cdot|)/2$. Then, the strain is decomposed as

$$\boldsymbol{\varepsilon}_\pm=\sum_{a=1}^{d}\langle\varepsilon_a\rangle_\pm\boldsymbol{n}_a\otimes\boldsymbol{n}_a \quad (4)$$

with d dimension of the domain Ω. $\boldsymbol{\varepsilon}_+$ and $\boldsymbol{\varepsilon}_-$ are tensile and compressive strains, respectively. ε_a is the principal strain and $\boldsymbol{n}_a$ is the direction of principal strain.

The phase field is assumed to only affect the tensile part of the elastic energy, thereby giving rise to

$$\psi(\boldsymbol{\varepsilon})=\left[(1-k)(1-\phi)^2+k\right]\psi^+(\boldsymbol{\varepsilon})+\psi^-(\boldsymbol{\varepsilon}) \quad (5)$$

with

$$\psi^\pm(\boldsymbol{\varepsilon})=\frac{\lambda}{2}\langle\mathrm{tr}(\boldsymbol{\varepsilon})\rangle_\pm^2+\mu\mathrm{tr}(\boldsymbol{\varepsilon}_\pm^2) \quad (6)$$

where $\psi^+(\boldsymbol{\varepsilon})$ and $\psi^-(\boldsymbol{\varepsilon})$ are tensile and compressive parts of the elastic energy. λ and μ are Lamé constants. In addition, $0 < k << 1$ is a parameter to avoid numerical singularity when $\phi = 1$.

Substituting Eqs. (3) and (5) into Eq. (1), one has

$$\begin{aligned}L(\boldsymbol{u},\Gamma)=&\int_\Omega\left\{\left[(1-k)(1-\phi)^2+k\right]\psi^+(\boldsymbol{\varepsilon})+\psi^-(\boldsymbol{\varepsilon})\right\}\mathrm{d}\Omega\\&+\int_\Omega\frac{G_c}{2l_0}\left(\phi^2+l_0^2\phi_{,i}\phi_{,i}\right)\mathrm{d}\Omega-\int_\Omega\boldsymbol{b}\cdot\boldsymbol{u}\mathrm{d}\Omega-\int_{\partial\Omega_h}\boldsymbol{t}\cdot\boldsymbol{u}\mathrm{d}S.\end{aligned} \quad (7)$$

The first variation of the energy functional L is then written as

$$\delta L = \int_\Omega \sigma_{ij}\delta u_{i,j}\mathrm{d}\Omega - \int_\Omega b_i\delta u_i\mathrm{d}\Omega - \int_{\partial\Omega_h} t_i\delta u_i\mathrm{d}S$$
$$-\int_\Omega 2(1-k)(1-\phi)\psi^+\delta\phi\mathrm{d}\Omega + \int_\Omega \frac{G_c}{l_0}\left(\phi\delta\phi + l_0^2\phi_{,i}\delta\phi_{,i}\right)\mathrm{d}\Omega, \tag{8}$$

where $\sigma_{ij} = \partial\psi/\partial\varepsilon_{ij}$.

According to the variational approach, $\delta L = 0$ stands for all admissible displacement and phase fields. Thus, Eq. (8) yields the equations:

$$\begin{cases} \sigma_{ij,j} + b_i = 0 \\ \left[\dfrac{2l_0(1-k)\psi^+}{G_c} + 1\right]\phi - l_0^2\phi_{,ii} = \dfrac{2l_0(1-k)\psi^+}{G_c}. \end{cases} \tag{9}$$

To ensure an accumulating phase field, a history field $H(\boldsymbol{x}, t)$ [15] is introduced:

$$H(\boldsymbol{x},t) = \max_{s\in[0,t]}\psi^+(\boldsymbol{\varepsilon}(\boldsymbol{x},s)) \tag{10}$$

with t the calculation time. Thus, the fracture propagation is driven by H instead of the tensile part of the elastic energy. The history field ensures the irreversibility condition of fractures under compression and unloading.

Replacing ψ^+ by H, the governing equations of strong form is written as

$$\begin{cases} \sigma_{ij,j} + b_i = 0 \\ \left[\dfrac{2l_0(1-k)H}{G_c} + 1\right]\phi - l_0^2\phi_{,ii} = \dfrac{2l_0(1-k)H}{G_c}. \end{cases} \tag{11}$$

The Neumann boundary conditions of Eq. (11) are given by

$$\sigma_{ij}n_j = t_i \quad \text{on } \partial\Omega_h, \tag{12}$$

$$\phi_i n_i = t_i \quad \text{on } \partial\Omega. \tag{13}$$

The Dirichlet boundary condition of Eq. (11) is given by

$$u_i = \bar{u}_i \quad \text{on } \partial\Omega_{h.} \tag{14}$$

3 Finite element implementation

The phase field modelling of fracture propagation is naturally a 2-field problem ($\boldsymbol{u}$ and ϕ). We use a conventional finite element method to solve the governing equations (11). Standard vector-matrix notation is used and the finite element discretization of the displacement and phase field is

$$\boldsymbol{u} = \boldsymbol{N}_u\hat{\boldsymbol{u}}, \quad \phi = \boldsymbol{N}_\phi\hat{\phi}, \tag{15}$$

where $\boldsymbol{N}_u$ and $\boldsymbol{N}_\phi$ are matrices involving the shape functions, and $\hat{\boldsymbol{u}}$ and $\hat{\phi}$ are vectors consisting of node values of the displacement and phase field. $\boldsymbol{N}_u$ and $\boldsymbol{N}_\phi$ are given by

$$\boldsymbol{N}_u = \begin{bmatrix} N_1^u & 0 & N_2^u & 0 & \cdots & N_n^u & 0 \\ 0 & N_1^u & 0 & N_2^u & \cdots & 0 & N_n^u \end{bmatrix}, \tag{16}$$

$$\boldsymbol{N}_\phi = \begin{bmatrix} N_1^\phi & N_2^\phi \cdots N_n^\phi \end{bmatrix} \tag{17}$$

where N_i^u and N_i^ϕ (are the shape functions of the displacement and phase field. n is the number of element nodes.

According to the finite element approximation, the weak form of the governing equations (11) gives rise to

$$\int_\Omega \boldsymbol{B}_u^{\mathrm{T}}\tilde{\boldsymbol{D}}\boldsymbol{B}_u\mathrm{d}\Omega\,\hat{\boldsymbol{u}} = \int_\Omega \boldsymbol{N}_u^{\mathrm{T}}\boldsymbol{b}\mathrm{d}\Omega + \int_{\partial\Omega}\boldsymbol{N}_u^{\mathrm{T}}\boldsymbol{t}\mathrm{d}\Omega, \tag{18}$$

$$\int_\Omega \left\{\boldsymbol{N}_\phi^{\mathrm{T}}\left[2(1-k)H + G_c/l_0\right]\boldsymbol{N}_\phi + \boldsymbol{B}_\phi^{\mathrm{T}}\mathrm{G_c}l_0\boldsymbol{B}_\phi\right\}\mathrm{d}\Omega\hat{\phi}$$
$$= \int_\Omega 2\boldsymbol{N}_\phi^{\mathrm{T}}(1-k)H\mathrm{d}\Omega. \tag{19}$$

where $\boldsymbol{B}_u$ and $\boldsymbol{B}_\phi$ are the gradient matrices of shape functions given by

$$\boldsymbol{B}_u = \begin{bmatrix} \dfrac{\partial N_1^u}{\partial x} & 0 & \cdots & \dfrac{\partial N_n^u}{\partial x} & 0 \\ 0 & \dfrac{\partial N_1^u}{\partial y} & \cdots & 0 & \dfrac{\partial N_n^u}{\partial y} \\ \dfrac{\partial N_1^u}{\partial y} & \dfrac{\partial N_1^u}{\partial x} & \cdots & \dfrac{\partial N_n^u}{\partial y} & \dfrac{\partial N_n^u}{\partial x} \end{bmatrix}, \tag{20}$$

$$\boldsymbol{B}_\phi = \begin{bmatrix} \dfrac{\partial N_1^\phi}{\partial x} & \dfrac{\partial N_2^\phi}{\partial x} & \cdots & \dfrac{\partial N_n^\phi}{\partial x} \\ \dfrac{\partial N_1^\phi}{\partial y} & \dfrac{\partial N_2^\phi}{\partial y} & \cdots & \dfrac{\partial N_n^\phi}{\partial y} \end{bmatrix}. \tag{21}$$

$\tilde{\boldsymbol{D}}$ is the degraded constitutive matrix, which can be derived from the elasticity tensor of fourth order $\boldsymbol{D} = \partial\boldsymbol{\sigma}/\partial\boldsymbol{\varepsilon}$. The matrix $\tilde{\boldsymbol{D}}$ is written as

$$\tilde{\boldsymbol{D}} = \begin{bmatrix} D_{1111} & D_{1122} & D_{1133} & D_{1112} & D_{1123} & D_{1113} \\ D_{2211} & D_{2222} & D_{2233} & D_{2212} & D_{2223} & D_{2213} \\ D_{3311} & D_{3322} & D_{3333} & D_{3312} & D_{3323} & D_{3313} \\ D_{1211} & D_{1222} & D_{1233} & D_{1212} & D_{1223} & D_{1213} \\ D_{2311} & D_{2322} & D_{2333} & D_{2312} & D_{2323} & D_{2313} \\ D_{1311} & D_{1322} & D_{1333} & D_{1312} & D_{1323} & D_{1313} \end{bmatrix} \tag{22}$$

with $D_{ijkl} = G_{ijkl}^v + G_{ijkl}^s$.

G_{ijkl}^v is calculated by

$$G_{ijkl}^v = \lambda\left\{[(1-k)(1-\phi)^2 + k]H_\varepsilon(tr(\boldsymbol{\varepsilon})) + H_\varepsilon(-tr(\boldsymbol{\varepsilon}))\right\}\delta_{ij}\delta_{kl} \tag{23}$$

where δ_{ij} and δ_{kl} are Kronecker deltas and $H_\varepsilon(x)$ is a Heaviside function:

$$H_\varepsilon(x) = \begin{cases} 1, x \geq 0 \\ 0, x < 0 \end{cases}. \tag{24}$$

According to the algorithm proposed by [17], G_{ijkl}^s is given by

$$G_{ijkl}^s = 2\mu\left\{\left[(1-k)(1-\phi)^2 + k\right]P_{ijkl}^+ + P_{ijkl}^-\right\} \tag{25}$$

with

$$P_{ijkl}^\pm = \sum_{a=1}^3\sum_{b=1}^3 H_\varepsilon(\varepsilon_a)\delta_{ab}n_{ai}n_{aj}n_{bk}n_{bl}$$
$$+\sum_{a=1}^3\sum_{b\neq a}^3\frac{1}{2}\frac{\langle\varepsilon_a\rangle_\pm - \langle\varepsilon_b\rangle_\pm}{\varepsilon_a - \varepsilon_b}n_{ai}n_{bj}(n_{ak}n_{bl} + n_{al}n_{bk}). \tag{26}$$

The implicit Generalized-α method [18] is used for time integration. In each time step, we adopt the staggered algorithm to solve the coupled equations (18) and (19). That means the displacement and phase field are solved independently. In addition, the Newton-Raphson method is used to conduct iterations on Eqs. (18) and (19).

4 Verification of the numerical simulation

4.1 Direct tension test

The first example used for verification of the numerical method is a pre-notched square plate subjected to tension loading. This benchmark test has been computed by Liu et al. [19] and Hesch and Weinberg [20] with the geometry and boundary conditions shown in Fig. 3. The width of the notch is l_0, and these parameters are used: $E = 210$ GPa, $\nu = 0.3$, and $G_c = 2700$ J/m^2. The length parameter $l_0 = 7.5 \times 10^{-3}$ mm and 1.5×10^{-2} mm, respectively. The plate has 64516 Q4 elements with size $h \approx 3.96 \times 10^{-3}$ mm.

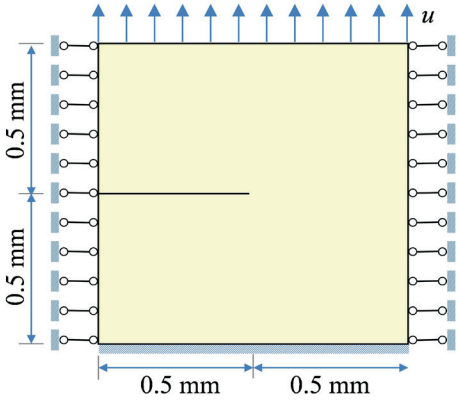

Fig. 3 Geometry and boundary condition of the pre-notched plate subjected to tension

A displacement increment $\Delta u = 1 \times 10^{-5}$ mm is used for the first 450 time steps and $\Delta u = 1 \times 10^{-6}$ mm for the remaining time steps. The final crack patterns for the two fixed length scale parameters l_0 are presented in Fig. 4, while the load-displacement curves on the top boundary of the plate are presented in Fig. 5. Both the final crack patterns and the load-displacement curves are in good agreement with the results of Hesch and Weinberg [20] and Liu et al. [19].

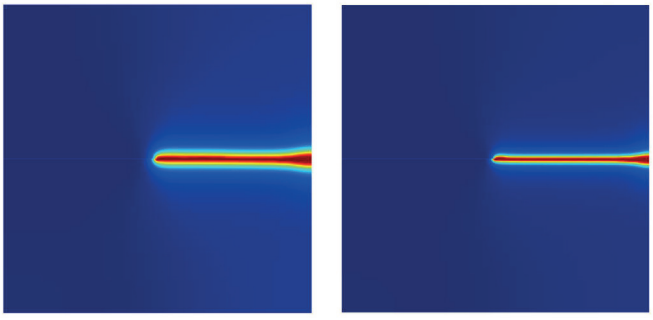

(a) $l_0 = 1.5 \times 10^{-2}$ mm (b) $l_0 = 7.5 \times 10^{-3}$ mm

Fig. 4 Final crack patterns of the pre-notched plate subjected to tension

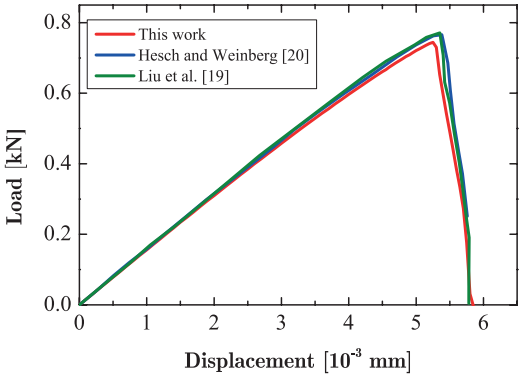

(a) $l_0 = 1.5 \times 10^{-2}$ mm

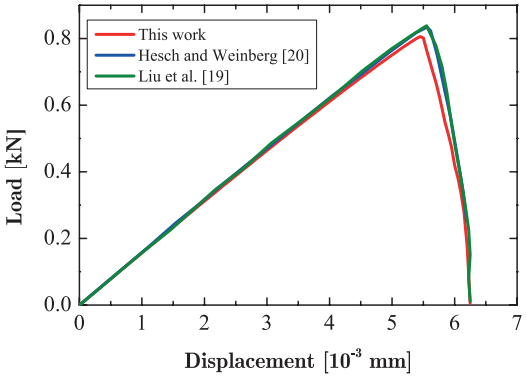

(b) $l_0 = 7.5 \times 10^{-3}$ mm

Fig. 5 Load-displacement curve of the pre-notched plate subjected to tension

4.2 Brazil splitting tests

In this example, we simulate the Brazil splitting tests on a cylinder rock specimen with no pre-existing notches. The specimen has a diameter of 100 mm, while these material parameters are used: $\rho = 2630$ kg/m^3, $E = 90$ GPa, $\nu = 0.3$, $G_c = 15$ J/m^2, and $l_0 = 2$ mm. A total of 24696 6-node quadratic elements are used to discretize the specimen with the maximum element size $h = 1$ mm.

The final crack pattern by using the phase field method is shown in Fig. 6a. A vertical propagating crack is observed and crack branching occurs close to the two ends of the specimen because of local compression. Fig. 6b presents a schematic diagram of the experimental results from [21, 22]. The crack pattern obtained by the phase field modeling is consistent with that of the experimental tests. This observation convinces the feasibility and practicability of the phase field method in modeling cracks in Brazilian discs.

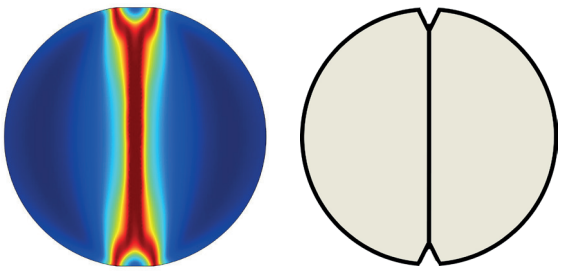

(a) (b)

Fig. 6 Final crack patterns of the Brazil splitting tests: (a) the phase field modeling, and (b) the schematic diagram of the experimental results

5 Brazilian discs with vertically arranged notches

5.1 Geometry and parameters

In this paper, we consider the Brazilian discs with vertically and horizontally arranged pre-existing notches. The discs have a diameter of 100 mm, and the geometric center of the notch set is consistent with that of the specimen. All the notches have a width of l_0 and a length of 20 mm. The inclination angle of the notches is 45. We define the spacing S as the distance between the centers of two adjoining notches. These material parameters are used: $\rho = 2630$ kg/m^3, $E = 120$ GPa, $v = 0.3$, $G_c = 1.42$ J/m^2, and $l_0 = 2$ mm. 6-node quadratic elements with the maximum element size $h = 1$ mm are used to discretize the specimen.

5.2 The influence of the number of notches

Figure 7 shows the final crack patterns of the discs with different numbers of vertically arranged pre-existing notches. The spacing between two notches is 2 cm. For only a single notch, the cracks initiate from the tips of the notch and propagate at a small angle with the direction of loading (Fig. 6a). If the number of notches is more than 1, outer cracks initiate from the notch tips and propagate at a small angel with the vertical direction, finally coalescing with the ends of the disc. The inner cracks initiate from the notch tips and coalesce with the center of an adjoining notch. These inner cracks propagate perpendicular to the notches (Fig. 6b, c, d).

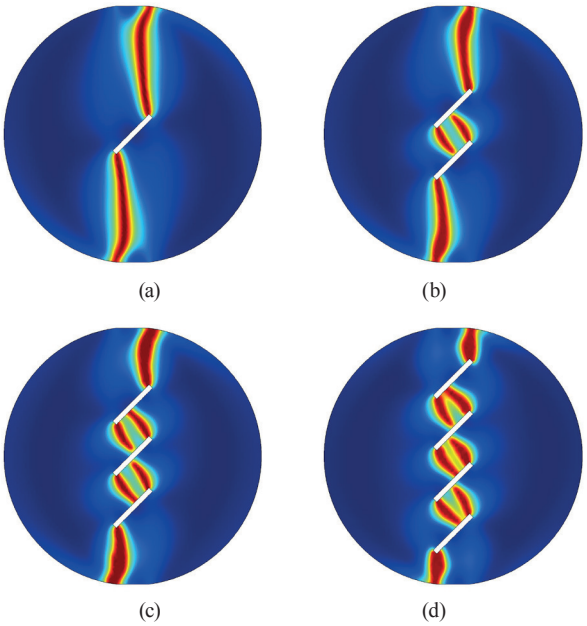

Fig. 7 Final crack patterns of the Brazilian discs with vertically arranged notches: (a) one notch, (b) two notches, (c) three notches, and (d) four notches

We compare the final crack patterns obtained by the phase field modeling with those obtained from DDM simulation [12], PFC simulation [13], and experimental tests [11]. The observations in Fig. 8 show that the results of the phase field modeling are in good agreement with the previous numerical simulations and experimental tests.

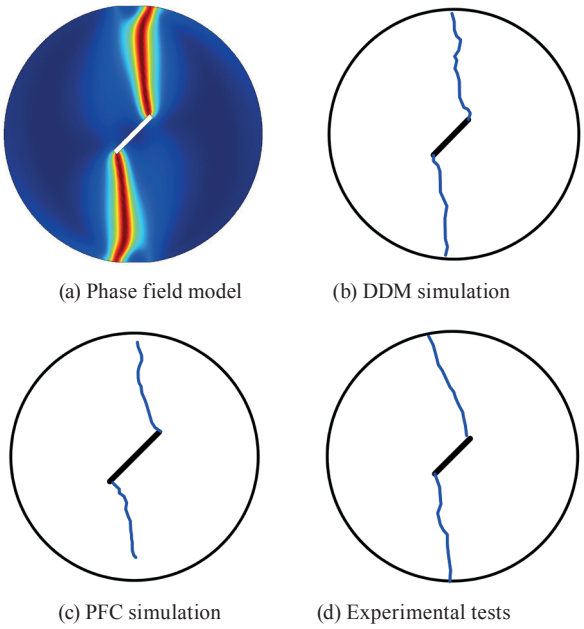

Fig. 8 Comparison of the crack patterns from the numerical simulations and experimental tests for one notch

Figure 9 presents the load-displacement curves of the specimen for different notch number. As observed, the peak load of the specimen decreases as the notch number increases. The increase of the vertically arranged notches leads to the decrease in the strength of the pre-notched Brazilian discs.

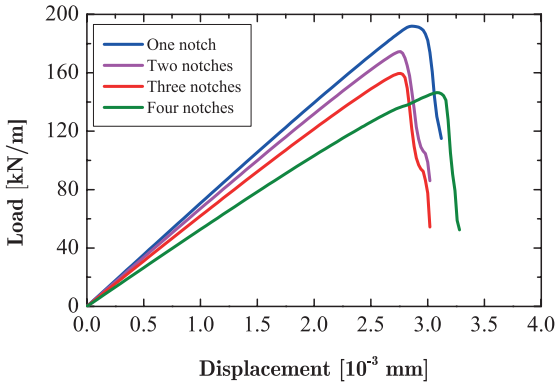

Fig. 9 Load-displacement curves of the Brazilian discs with vertically arranged notches

5.3 The influence of the spacing

To specify the influence of the spacing S, we set the spacing S as 2 cm, 3 cm, and 4 cm for the Brazilian discs with two pre-existing notches and $S = 1$ cm, 2cm, and 3cm for the Brazilian discs with three pre-existing notches. Figure 10 presents the final crack patterns of the Brazilian discs with two vertically arranged notches under different spacing. The outer cracks initiating from the tips of the notches are similar. The distance between two inner cracks decreases as the notch spacing increase. When the spacing is 4 cm, the two inner cracks from the inner tips of the notches coalesce.

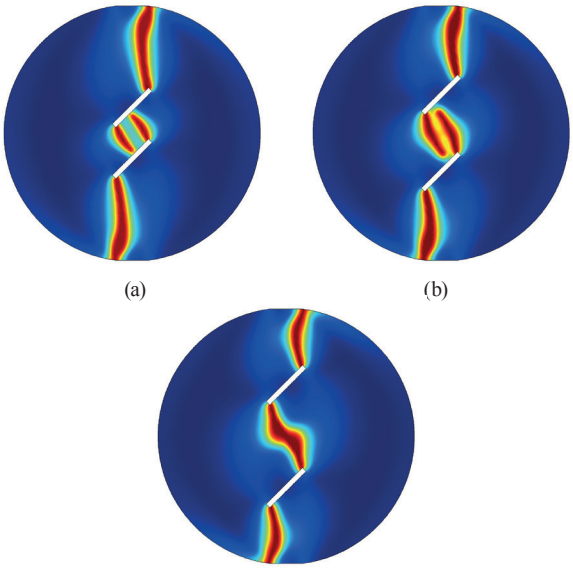

Fig. 10 Final crack patterns of the Brazilian discs with two vertically arranged notches: (a) $S = 2$ cm, (b) $S = 3$ cm, and (c) $S = 4$ cm

Figure 11 presents the final crack patterns of the Brazilian discs with three vertically arranged notches under different notch spacing. The outer cracks initiating from the tips of the notches are similar to those in the Brazilian discs with two notches. When $S = 1$ cm, only one inner crack occurs between two adjoining notches. When the spacing is 3 cm, the two inner cracks from the inner tips of the notches coalesce.

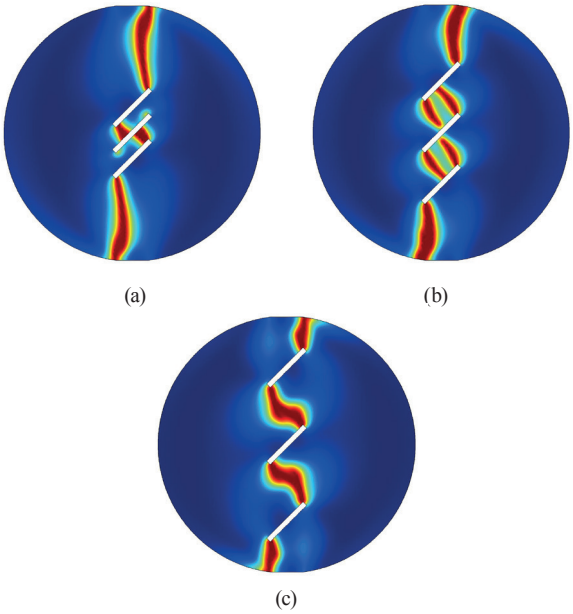

Fig. 11 Final crack patterns of the Brazilian discs with three vertically arranged notches: (a) $S = 1$ cm, (b) $S = 2$ cm, and (c) $S = 3$ cm

Figure 12 shows the influence of spacing on the peak load for the Brazilian discs with two and three vertically arranged notches. As observed, the spacing has little influence on the peak load. That is, the strength of the Brazilian disc is not sensitive to the variation in the notch spacing. This observation is different from that obtained by the PFC simulations [13].

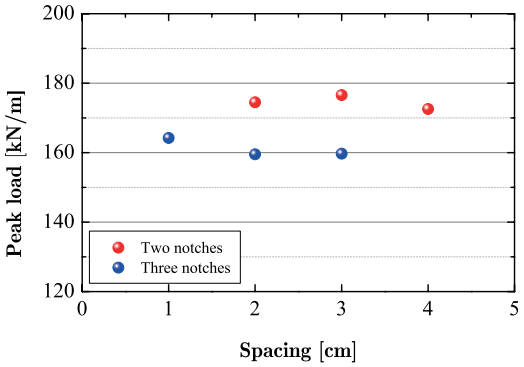

Fig. 12 Peak load of the Brazilian discs with two and three vertically arranged notches under different notch spacing

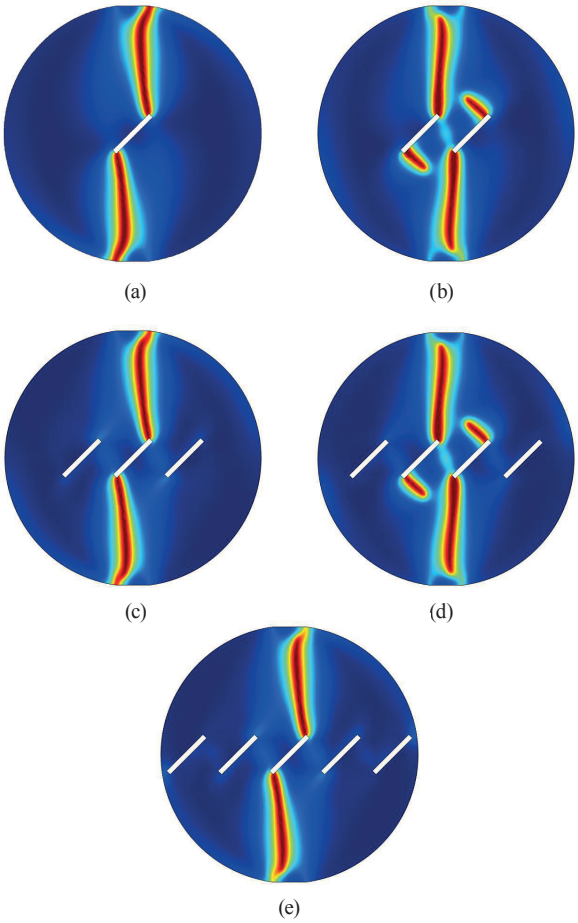

Fig. 13 Final crack patterns of the Brazilian discs with horizontally arranged notches: (a) one notch, (b) two notches, (c) three notches, (d) four notches, and (e) five notches

6 Brazilian discs with horizontally arranged notches

6.1 The influence of the number of notches

Figure 13 shows the final crack patterns of the Brazilian discs with different numbers of horizontally arranged pre-existing notches. The spacing between two notches is 2 cm. When the notch number is 1, 3, and 5, the crack patterns are similar. Outer tensile cracks initiate from the tips of the middle notch and propagate at a small angle with the direction of loading (Fig. 13a, c, e).

The crack patterns are similar in the cases of two and four notches. Cracks initiate and propagate only from the tips of

the two notches in the disc center. Except the crack along the loading direction, another inner crack is observed to initiate from the other tip of a notch. The inner tensile crack is perpendicular to the notch (Fig. 13b, d).

Figure 14 presents the load-displacement curves of the specimen with horizontally arranged notches under different notch number. As observed, the specimen has a decreasing peak load as the pre-existing notch increases. An obvious decrease in the strength of the pre-notched Brazilian discs is shown for four and five notches.

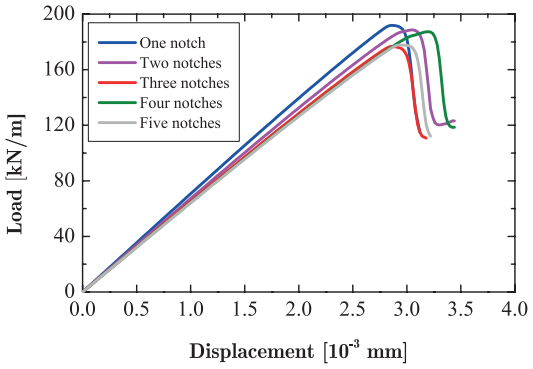

Fig. 14 Load-displacement curves of the Brazilian discs with horizontally arranged notches

6.2 The influence of the spacing

We also present the influence of the spacing on the crack initiation and propagation of the Brazilian discs with horizontally arranged notches. We set the spacing S = 2 cm, 3 cm, and 4 cm for the Brazilian discs with two pre-existing notches, afterwards, S = 1 cm, 2cm, and 3cm for the Brazilian discs with three pre-existing notches. Figure 15 presents the final crack patterns of the Brazilian discs with two horizontally arranged notches under different spacing. When S = 2 cm and S = 3 cm, the crack patterns are similar. Outer tensile cracks initiate from the notch tips and coalesce with the end of the specimen. When S = 4 cm, outer cracks initiate from the notch tips. However, the length of the outer crack is smaller than that of the inner crack and new cracks initiate close to the initial outer cracks and coalesce with the ends of the specimen.

Figure 16 presents the final crack patterns of the Brazilian discs with three horizontally arranged notches under different notch spacing. When S = 2 cm and S = 3 cm, the crack patterns are similar. Only two outer cracks are obtained and coalesce with the two ends of the specimen. When S = 1 cm, except the out cracks, inner cracks initiate from the notches and propagate between two adjoining notches.

Figure 17 shows the influence of spacing on the peak load of the Brazilian discs with two and three horizontally arranged notches. As observed, the peak load increases as the notch spacing increases. That is, a larger strength of the Brazilian disc is obtained for a larger spacing between two notches because the notches are placed farther from the centre of the disc where stress concentration occurs.

This observation is different from that obtained by the PFC simulations [13]. In addition, the peak load decreases as the notches increase at a fixed spacing.

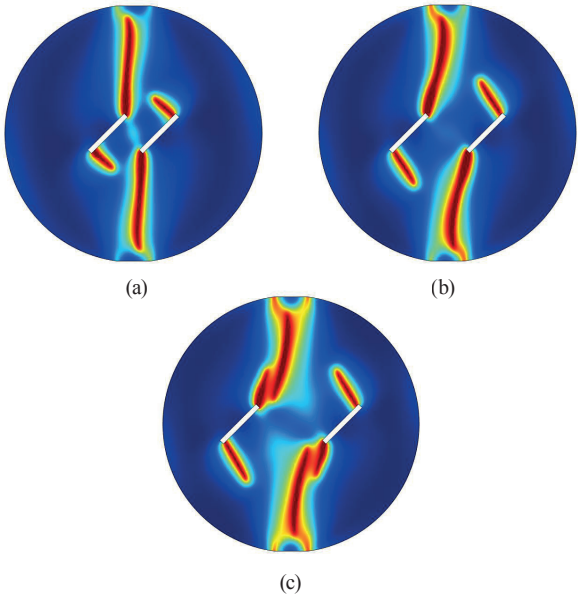

Fig. 15 Final crack patterns of the Brazilian discs with two horizontally arranged notches: (a) S = 2 cm, (b) S = 3 cm, and (c) S = 4 cm

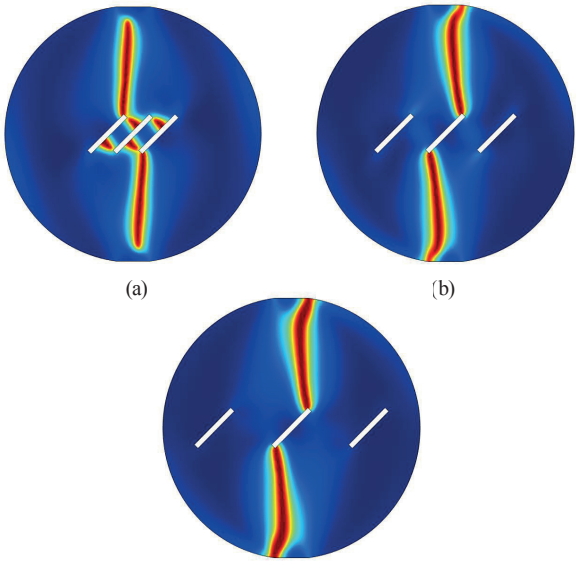

Fig. 16 Final crack patterns of the Brazilian discs with three horizontally arranged notches: (a) S = 1 cm, (b) S = 2 cm, and (c) S = 3 cm

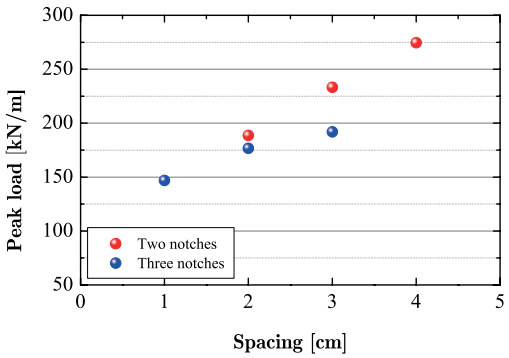

Fig. 17 Peak load of the Brazilian discs with two and three horizontally arranged notches under different notch spacing

7 Conclusions

In this paper, the crack propagation in the Brazilian discs with multiple pre-existing notches is investigated by using a phase field method. The phase field method (PFM) uses a smeared zone to model the sharp cracks without any external fracture criteria. The phase field modelling in this paper is verified by using a direct tension test and an indirect splitting test on a Brazilian specimen with no pre-existing notches where the simulated results are in good agreement with previous numerical and experimental results.

The influence of the notch number and spacing on the crack propagation in the Brazilian discs with multiple vertically and horizontally arranged notches is studied. The final crack patterns obtained by the phase field modelling are consistent with those of previous numerical simulations and experimental tests, such as DDM and PFC. For a Brazilian disc with vertically arranged notches, outer cracks initiate from the notch tips and propagate at a small angle with the vertical direction, finally coalescing with the ends of the disc. Inner cracks initiate from the other notch tips and coalesce with the center of an adjoining notch. The strength of the specimen decreases as the notch number increases. The increase in the notch spacing leads to the decrease in the spacing between two inner cracks, which coalesce when the spacing is too small. In addition, the notch spacing has little influence on the peak load of the discs with vertically arranged notches. For the Brazilian discs with horizontally arranged pre-existing notches, only outer cracks initiate when the notch number is 1, 3, and 5. For two and four notches, both outer and inner cracks initiate. The Brazilian discs have a decreasing peak load as the pre-existing notches increase. The peak load of the Brazilian discs containing horizontally arranged notches increases as the notch spacing increases.

The presented numerical results are expected to increase the understanding of crack initiation, propagation, and coalescence in rock tests and can be a preference for the stability in rock engineering where pre-existing fractures are a crucial factor for safety, such as tunnelling, slope, hydraulic fracturing, and explosive engineering. In addition, the presented numerical simulation in this paper can be extended to analyse complex dynamic crack patterns in Brazilian discs with multiple notches in future research, such as multiple crack branching. Some novel and more effective methods (e.g. the hybrid XFEM-phase field method [23]) will be also applied in modelling fractures in the pre-notched Brazilian discs.

Acknowledgement

The financial support provided by the Sino-German (CSC-DAAD) Postdoc Scholarship Program 2016 is gratefully acknowledged.

References

[1] Chen, C. H., Chen, C. S., Wu, J. H. "Fracture toughness analysis on crackedring disks of anisotropic rock". *Rock Mechanics and Rock Engineering*, 41(4), pp. 539–562. 2008. 10.1007/s00603-007-0152-9

[2] Lee, H., Jeon, S. "An experimental and numerical study of fracturecoalescence in pre-cracked specimens under uniaxial compression". *International Journal of Solids and Structures*, 48(6), pp. 979–999. 2011. 10.1016/j.ijsolstr.2010.12.001

[3] Park, C. H., Bobet, A. "Crack coalescence in specimens with open andclosed flaws: a comparison". *International Journal of Rock Mechanics and Mining Sciences*, 46(5), pp. 819–829. 2009. 10.1016/j.ijrmms.2009.02.006

[4] Sagong, M., Bobet, A. "Coalescence of multiple flaws in a rock-modelmaterial in uniaxial compression". *International Journal of Rock Mechanics and Mining Sciences*, 39(2), pp. 229–241. 2002. 10.1016/S1365-1609(02)00027-8

[5] Wong, L., Einstein, H. "Crack coalescence in molded gypsum and carrara marble: Part 1. macroscopic observations and interpretation". *Rock Mechanics and Rock Engineering*, 42(3), pp. 475–511. 2009. 10.1007/s00603-008-0002-4

[6] Chong, K. P., Kuruppu, M. "New specimen for fracture toughness determination for rock and other materials". *International Journal of Fracture*, 26(2), pp. R59–R62. 1984. 10.1007/BF01157555

[7] Dai, F., Xia, K., Zheng, H., Wang, Y. X. "Determination of dynamic rock mode-I fracture parameters using cracked chevron notched semi-circular bend specimen". *Engineering fracture mechanics*, 78(15), pp. 2633–2644. 2011. 10.1016/j.engfracmech.2011.06.022

[8] Zhou, X. P., Wang, Y. T. "Numerical simulation of crack propagation andcoalescence in pre-cracked rock-like brazilian disks using the non-ordinarystate-based peridynamics". *International Journal of Rock Mechanics and Mining Sciences*, 89, pp. 235–249. 2016. 10.1016/j.ijrmms.2016.09.010

[9] Atkinson, C., Smelser, R., Sanchez, J. "Combined mode fracture via thecracked Brazilian disk test". *International Journal of Fracture*, 18(4):279–291. 1982. 10.1007/BF00015688

[10] Haeri, H., Shahriar, K., Marji, M. F., Moarefvand, P. "Experimental andnumerical study of crack propagation and coalescence in pre-crackedrock-like disks". *International Journal of Rock Mechanics and Mining Sciences*, 67, pp. 20–28. 2014. 10.1016/j.ijrmms.2014.01.008

[11] Haeri, H., Khaloo, A., Marji, M. F. "Experimental and numerical analysis of Brazilian discs with multiple parallel cracks." *Arabian Journal of Geosciences*, 8(8), pp. 5897–5908. 2015. 10.1007/s12517-014-1598-1

[12] Sarfarazi, V., Haeri, H., Fatehi, M. "Fracture Mechanism of Brazilian Discs with Multiple Parallel Notches Using PFC2D". *Periodica Polytechnica Civil Engineering*, 61(4), pp. 1–11. 2017. 10.3311/PPci.10310

[13] Robertson, B. A. "Phase Field Fracture Mechanics MAE 523 Term Paper". *Arizona University*, pp. 1–24. 2015. http://prod.sandia.gov/techlib/access-control.cgi/2015/1510305r.pdf

[14] Francfort, G. A., Marigo, J. J. "Revisiting brittle fracture as an energy minimization problem". *Journal of the Mechanics and Physics of Solids*, 46(8), pp. 1319–1342.1998. https://doi.org/10.1016/S0022-5096(98)00034-9

[15] Miehe, C., Hofacker, M., Welschinger, F. "A phase field model for rate-independent crack propagation: Robust algorithmic implementation based on operator splits". *Computer Methods in Applied Mechanics and Engineering*, 199(45), pp. 2765–2778. 2010. 10.1016/j.cma.2010.04.011

[16] Miehe, C., Welschinger, F., Hofacker, M. "Thermodynamically consistent phase-field models of fracture: Variational principles and multi-field FE implementations". *International Journal for Numerical Methods in Engineering*, 83(10), pp. 1273–1311. 2010. 10.1002/nme.2861

[17] Miehe, C. "Comparison of two algorithms for the computation of fourth-order isotropic tensor functions". *Computers & structures*, 66(1), pp. 37–43. 1998. 10.1016/S0045-7949(97)00073-4

[18] Borden, M. J., Verhoosel, C. V., Scott, M. A., Hughes, T. J., Landis, C. M. "A phase-field description of dynamic brittle fracture". *Computer Methods in Applied Mechanics and Engineering*, 217–220, pp. 77–95. 2012. 10.1016/j.cma.2012.01.008

[19] Liu, G., Li, Q., Msekh, M. A., Zuo, Z. "Abaqus implementation of monolithic and staggered schemes for quasi-static and dynamic fracture phase-field model". *Computational Materials Science*, 121, pp. 35–47.2016. 10.1016/j.commatsci.2016.04.009

[20] Hesch, C., Weinberg, K. "Thermodynamically consistent algorithms for a finite-deformation phase-field approach to fracture". *International Journal for Numerical Methods in Engineering*, 99(12), pp. 906–924. 2014. 10.1002/nme.4709

[21] Feng, K. N., Ruan, D., Pan, Z., Collins, F., Bai, Y., Wang, C. M., Duan, W. H. "Effect of strain rate on splitting tensile strength of geopolymer concrete". *Magazine of concrete research*, 66(16), pp. 825–835.2014. 10.1680/macr.13.00322

[22] Proveti, J. R. C.,Michot, G. "The Brazilian test: a tool for measuring the toughness of a material and its brittle to ductile transition". *International journal of fracture*, 139(3), pp. 455–460. 2006. 10.1007/s10704-006-0067-6

[23] Giovanardi, B., Scotti, A., Formaggia, L. "A hybrid XFEM–Phase field (Xfield) method for crack propagation in brittle elastic materials". *Computer Methods in Applied Mechanics and Engineering*, 320(15), pp. 396–420. 2017. 10.1016/j.cma.2017.03.039